Mitochondrial Network Branching Enables Rapid Protein Spread with Slower Mitochondrial Dynamics

Prabha Chuphal, Jordan D. Lanctôt, Sean P. Cornelius, and Aidan I. Brown*
Department of Physics, Toronto Metropolitan University, Toronto M9N 1B4, Canada

(Received 13 May 2024; accepted 16 September 2024; published 22 October 2024)

Mitochondrial network structure is controlled by the dynamical processes of fusion and fission, which merge and split mitochondrial tubes into structures including branches and loops. To investigate the impact of mitochondrial network dynamics and structure on the spread of proteins and other molecules through mitochondrial networks, we used stochastic simulations of two distinct quantitative models that each included mitochondrial fusion and fission, and particle diffusion via the network. Better-connected mitochondrial networks and networks with faster dynamics exhibit more rapid particle spread on the network, with little further improvement once a network has become well connected. As fragmented networks gradually become better connected, particle spread either steadily improves until the networks become well connected for slow-diffusing particles or plateaus for fast-diffusing particles. We compared model mitochondrial networks with both end-to-end and end-to-side fusion, which form branches, to nonbranching model networks that lack end-to-side fusion. To achieve the optimum (most rapid) spread that occurs on well-connected branching networks, nonbranching networks require much faster fusion and fission dynamics. Thus, the process of end-to-side fusion, which creates branches in mitochondrial networks, enables rapid spread of particles on the network with relatively slow fusion and fission dynamics. This modeling of protein spread on mitochondrial networks builds toward mechanistic understanding of how mitochondrial structure and dynamics regulate mitochondrial function.

DOI: 10.1103/PRXLife.2.043005

I. INTRODUCTION

Mitochondria are highly dynamic organelles with multiple important functions [1,2], notably, production of adenosine triphosphate (ATP) via oxidative phosphorylation [3]. Mitochondrial dysfunction is connected to several diseases, such as diabetes, cancer, and Parkinson's disease, among others [4–7]. While often depicted as bean-shaped puncta, mitochondrial fusion and fission dynamics allow formation of mitochondrial tubes of a range of sizes [8]. End-to-side mitochondrial fusion forms three-way junctions that branch mitochondrial tubes, allowing mitochondria to form extended network structures that include loops [9–11]. Mitochondrial dynamics are important to mitochondrial quality control and function [12], as well as to cell metabolism [13], motion [14], and differentiation [15].

The level of connectivity for tubular mitochondria is controlled by both fission and fusion events [16–19], as well as organelle movement [20–22]. Relatively frequent fission leads to more fragmented and bean-like mitochondria, while relatively frequent fusion leads to a more connected and tubular mitochondrial network. Mitochondria in yeast cells can be well connected, with a mean of two mitochondrial fragments and most mitochondrial mass part of a relatively large mitochondrial fragment [9]; mitochondrial fragments in mammalian cells can take a range of sizes from large to small [8]; while in plant cells mitochondria are typically many small bean-like fragments [23]. In cells with relatively tubular mitochondria, network connectivity can be adjusted by changes to metabolism and cell stress [24–30]. Various hypotheses have been explored to explain why mitochondria in certain cell types form extended and dynamic connected networks [31,32], including to share proteins and other molecules [33], undergoing fission to provide growing and dividing cells with sufficient numbers of mitochondria [34], and to help separate poorly functioning mitochondria to be removed by the mitophagy quality control pathway [1,12].

We will focus on how mitochondrial network connectivity and dynamics in cells with relatively tubular (rather than bean-like) mitochondria facilitate the sharing of proteins and other molecules, which appears key to providing mitochondria in these cells with a full protein complement. Low mRNA copy number, cotranslational delivery, and stochastic targeting to mitochondria can lead some mitochondrial fragments to directly receive few copies of specific nuclear-encoded [35] proteins; these proteins could instead be provided following fusion with another fragment [36,37]. With limited mitochondrial DNA error-correction mechanisms, mutation levels of genes encoded on mitochondrial DNA are relatively high [38]. While proteins produced in one mitochondrial fragment may be dysfunctional, functional proteins produced in another fragment can be shared following fusion, known as complementation [39]. While fusing all mitochondria together into one network may facilitate rapid sharing, this could hamper the distribution of mitochondria throughout the cell and may pose challenges for other purposes served by mitochondrial dynamics [32].

*Contact author: aidan.brown@torontomu.ca

Recently developed experimental techniques enable measurement of many aspects of mitochondria [29,37,40–42], providing a quantitative basis to model mitochondrial networks and processes, including those important to sharing proteins among mitochondria. Modeling work for mitochondrial network structure has outlined how a balance between fusion and fission leads to critical mitochondrial networks near the percolation threshold [8,43,44], how mitochondrial motion along filaments is key to spatially organizing mitochondrial networks [45], and very recent work explored how kinetics and mechanics control spatial mitochondrial network morphology and found high dependence of morphology and rearrangement timescales on fission and fusion rates [19].

To investigate how mitochondrial network structure and dynamics—particularly branching of networks—affect protein spread, we simulate two different stochastic models of mitochondrial networks, one on a two-dimensional spatial lattice and a second agent-based aspatial model. This work builds on related modeling of how mitochondrial structure affects protein spread on mitochondrial networks, including static [9,10] and dynamic networks [21,31,37,46], as well as earlier calculations for transitions on fluctuating disordered lattices [47–52]. Among many similarities, the particle spread behavior of both models we apply suggests that the branching of mitochondrial networks allows for rapid spread with much slower mitochondrial dynamics compared to networks without branching.

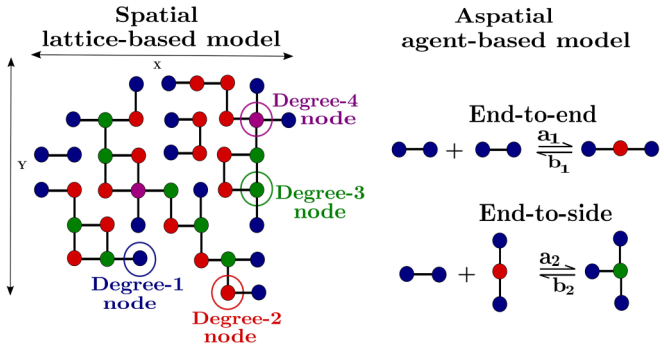

FIG. 1. Schematic representing two mitochondrial network models. Left: Spatial lattice-based model with mitochondria represented by nodes on a two-dimensional lattice. Neighboring nodes connect (fuse) at rate λ_{add} and disconnect (fission) at rate λ_{remove}. Right: Aspatial agent-based model with each minimal mitochondrial fragment represented by two permanently connected nodes. Two free mitochondrial ends (only joined to permanently connected partner) end-to-end fuse into a degree-two node with rate a_1 and a degree-two node end-to-end fissions into two free ends with rate b_1; a free end and degree-two node end-to-side fuse into a degree-three node with rate a_2 and a degree-three node end-to-side fissions into a free end and a degree-two node with rate b_2. For both panels, node color indicates node degree.

II. RESULTS

A. Two-dimensional lattice-based model

We first explore a mitochondrial network model with stochastic fusion and fission between mitochondrial units embedded on a two-dimensional lattice (see Fig. 1, left panel), following earlier work that analyzed a similar model with both mean-field calculations and stochastic simulations [31]. Although mitochondrial networks are embedded in a three-dimensional volume and in many cell types are found well spread through the three-dimensional space, in several well-studied cell types the spatial arrangement of mitochondria is approximately two-dimensional, such as mitochondria in flat cells [21] or mitochondria that form a layer just inside the yeast cell membrane [9]. Analysis of mitochondrial networks, with percolation exponents closer to those expected for two dimensions than three dimensions [44], also suggests consideration of two-dimensional mitochondrial networks.

In this model, neighboring nodes on a square lattice connect (fuse) at rate λ_{add} and disconnect (fission) at rate λ_{remove}, such that neighboring mitochondria are connected with probability $p = \lambda_{\text{add}}/(\lambda_{\text{add}} + \lambda_{\text{remove}})$, and $\tau = 1/(\lambda_{\text{add}} + \lambda_{\text{remove}})$ is the timescale of network dynamics. A particle at a node moves to neighboring connected nodes with a rate of one, setting the simulation timescale. On a fully connected network, a particle can move on the network with effective diffusivity D_{eff} equal to the particle diffusivity $D = 1$. For an incomplete network, the particle would be unable to step across missing connections, so $D_{\text{eff}} < D$. The network dynamics and particle motion are simulated using the Gillespie algorithm [53]. For $\tau = 0$ connections between neighboring nodes fluctuate infinitely quickly and the status of each connection is not tracked—instead, when a particle attempts to cross to another node the particle is allowed to cross with probability p. For $\tau = \infty$ each connection is initially present with probability p, with no further network dynamics.

Figure 2(a) shows that the effective diffusivity increases as the connection probability p increases, recapitulating earlier work from stochastic simulations [31] and mean-field calculations on a fluctuating disordered lattice [31,47,48]. For small p the network mostly contains small node islands or isolated nodes, while for large p most nodes are connected into a single component [Fig. 2(a) insets]. With $\tau = 1/(\lambda_{\text{add}} + \lambda_{\text{remove}})$ the timescale of network dynamics, fast dynamics (small τ) leads the effective diffusivity to increase close to linearly with increasing connection probability p, with faster dynamics more linear with a higher D_{eff} at a given p. For infinitely fast dynamics $\tau \to 0$ each attempted step by the particle occurs with probability p, uncorrelated with previous steps. For slow dynamics (large τ) the effective diffusivity increases very little below the two-dimensional percolation threshold [54] $p = 0.5$ and rapidly rises above $p = 0.5$. This reflects the longer lifetime of connections and disconnections, such that successful and unsuccessful attempted steps become increasingly correlated in time. For $\tau \to \infty$ the network is frozen, with no changes in connections. For $\tau \to \infty$, Fig. 2(a) shows the effective diffusivity does not quite reach zero at and immediately below $p = 0.5$ due to the finite system simulated, while the effective diffusivity would sharply depart from zero at this threshold on an infinite network [31,47,48,54].

Complementing the effective diffusivity of Fig. 2(a), Fig. 2(b) shows the time to first arrive at a target node in the network, the mean first-passage time (MFPT), with randomly selected initial and target nodes. The MFPT decreases with increasing connection probability p, with shorter MFPT for

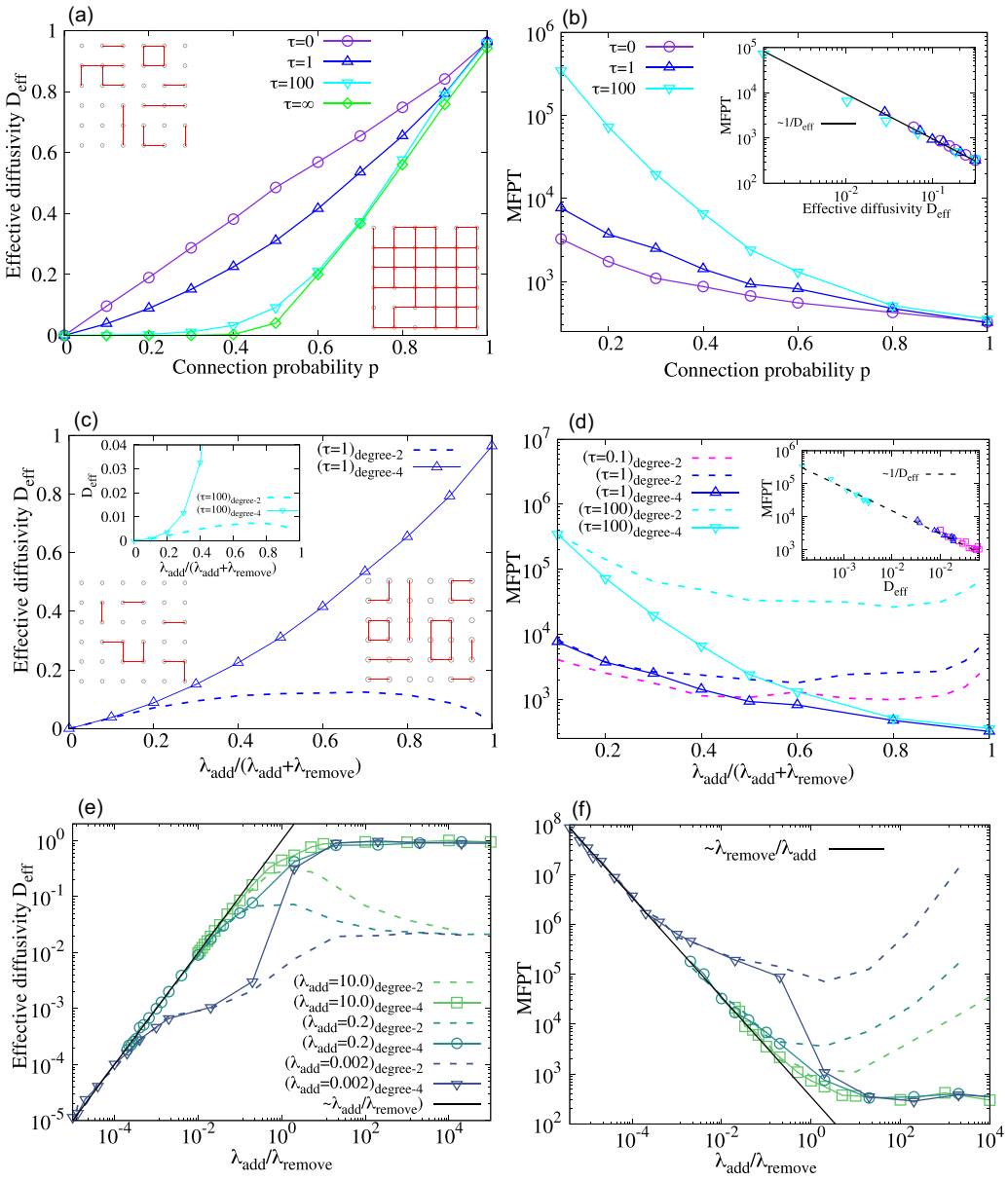

FIG. 2. Effective diffusivity and search time for particle diffusing on model dynamic mitochondrial networks on a two-dimensional lattice. (a) The effective diffusivity D_{eff} as connection probability p is varied. Legend indicates network dynamics timescale τ. Insets show typical networks for $p = 0.2$ and $p = 0.9$. (b) The MFPT of a diffusing particle to find a randomly selected lattice site from initial position at another randomly selected lattice site, as connection probability p is varied. Inset shows MFPT vs. D_{eff} from main plots of (a) and (b). Main plot legend, indicating τ, also applies to inset, with inset black line indicating MFPT $\sim 1/D_{\text{eff}}$ trend. In (a) and (b) nodes are permitted to connect to all four nearest neighbors. In (c)–(f), solid curves are for networks that permit nodes to connect to all four nearest neighbors (degree 4), and dashed curves indicate networks that permit nodes to connect to a maximum of two nearest neighbors (degree 2), as indicated in legends. (c) D_{eff} as fusion fraction of dynamics $\lambda_{\text{add}}/(\lambda_{\text{add}} + \lambda_{\text{remove}})$ is varied. The main plot is for $\tau = 1$ and inset is for $\tau = 100$. Insets in the main plot show typical networks for $p = 0.17$ and $p = 0.46$. (d) MFPT of a diffusing particle to find a randomly selected lattice site from initial position at another randomly selected lattice site, as $\lambda_{\text{add}}/(\lambda_{\text{add}} + \lambda_{\text{remove}})$ is varied. Legend indicates τ. Inset shows degree-2 MFPT vs. D_{eff} from main plots of (c) and (d). Main plot legend also applies to inset, with inset black curve indicating MFPT $\sim 1/D_{\text{eff}}$ trend. (e) D_{eff} as balance between fusion and fission $\lambda_{\text{add}}/\lambda_{\text{remove}}$ is varied. Legend indicates fusion rate λ_{add} and black curve is $\sim\lambda_{\text{add}}/\lambda_{\text{remove}}$ trend. Legend entries for simulation data (those with λ_{add} values) in (e) also apply to (f). (f) MFPT as $\lambda_{\text{add}}/\lambda_{\text{remove}}$ is varied. Black curve is $\sim\lambda_{\text{remove}}/\lambda_{\text{add}}$ trend. Across all panels, particle diffusivity $D = 1$, the lattice is 21×21 with nodes on a square grid with intervals of one, and data averaged over 100 samples.

faster dynamics (smaller τ). The MFPT for large τ decreases by multiple orders of magnitude as p increases from 0.1 to 1 because for low p the particle must wait for fusion events to enable movement to new nodes, and τ represents this waiting time for a given pair of neighboring mitochondria. In contrast, the MFPT for small τ (including the infinitely fast dynamics of $\tau = 0$) decreases by approximately an order of magnitude from $p = 0.1$ to $p = 1$ as the search is slowed by low p due to less connectivity, rather than long waiting times for dynamics. As the effective diffusivity is essentially the probability for

the particle to successfully step from one mitochondria to another, allowing the particle to proceed on a search, the MFPT inversely scales with the effective diffusivity [Fig. 2(b) inset]. Figure 7 in the Appendix shows a sample particle trajectory for low, medium, and high connection probability p.

The results of Figs. 2(a) and 2(b) permit mitochondrial nodes on the two-dimensional lattice to connect to all four of their nearest neighbors, allowing degree-four nodes. We now examine how restricting the maximum node degree to below four impacts diffusion and search. On networks with such a restriction, the connection probability $p \neq \lambda_{\text{add}}/(\lambda_{\text{add}} + \lambda_{\text{remove}})$, as a fourth connection to a particular node cannot form. For networks with a maximum node degree of three (approximately as observed in mitochondrial networks [9]), the effective diffusivity D_{eff} and MFPT are qualitatively similar to networks permitting degree-four nodes, with monotonic changes in both quantities (see Fig. 9 in the Appendix). Restricting to a maximum node degree of three lowers the effective diffusivity and raises the MFPT compared to degree-four networks for better-connected networks with larger $\lambda_{\text{add}}/(\lambda_{\text{add}} + \lambda_{\text{remove}})$.

In contrast, networks with a maximum node degree of two exhibit qualitative distinctions in effective diffusivity and search behavior compared to networks permitting degree-three and degree-four nodes [Figs. 2(c) and 2(d)]. Such networks with a maximum node degree of two represent hypothetical mitochondrial networks without end-to-side fusion or the associated network branching. For low $\lambda_{\text{add}}/(\lambda_{\text{add}} + \lambda_{\text{remove}}) \lesssim 0.2$ the effective diffusivity D_{eff} for networks permitting maximum degree-two nodes is similar to the D_{eff} with degree-four nodes [Fig. 2(c)]. For $\lambda_{\text{add}}/(\lambda_{\text{add}} + \lambda_{\text{remove}}) \gtrsim 0.2$ the D_{eff} for maximum degree-two networks increases much more slowly as $\lambda_{\text{add}}/(\lambda_{\text{add}} + \lambda_{\text{remove}})$ increases than for degree-four networks. Although D_{eff} for degree-four networks monotonically increases with $\lambda_{\text{add}}/(\lambda_{\text{add}} + \lambda_{\text{remove}})$, for high $\lambda_{\text{add}}/(\lambda_{\text{add}} + \lambda_{\text{remove}}) \gtrsim 0.7$ the D_{eff} for maximum degree-two networks decreases with higher $\lambda_{\text{add}}/(\lambda_{\text{add}} + \lambda_{\text{remove}})$. Larger $\tau = 1/(\lambda_{\text{add}} + \lambda_{\text{remove}})$, representing slower network rearrangement, leads to greater difference between degree-four and degree-two D_{eff} [Fig. 2(c) main plot compared with inset plot].

Consistent with the trend for effective diffusivity, Fig. 2(d) shows similar and decreasing MFPT for degree-four and degree-two networks for small and increasing $\lambda_{\text{add}}/(\lambda_{\text{add}} + \lambda_{\text{remove}})$, higher MFPT for degree-two than degree-four networks at intermediate $\lambda_{\text{add}}/(\lambda_{\text{add}} + \lambda_{\text{remove}})$, and increasing MFPT for degree-two networks for high and increasing $\lambda_{\text{add}}/(\lambda_{\text{add}} + \lambda_{\text{remove}})$ values. The difference between degree-four and degree-two MFPT also increases with larger τ. The inset of Fig. 2(d) shows a MFPT $\sim D_{\text{eff}}^{-1}$ relationship for degree-two networks consistent with the relationship found in the inset of Fig. 2(b) for degree-four networks. Similar results to Figs. 2(a) and 2(c) are found for a larger lattice (see Fig. 8 in the Appendix).

Particles have similar effective diffusivity and MFPT on networks with degree-four or maximum of degree-two nodes for small $\lambda_{\text{add}}/(\lambda_{\text{add}} + \lambda_{\text{remove}})$ because in this low-connectivity regime limiting node degree to a maximum of two affects few nodes, as they are already largely disconnected [see left network insets of Figs. 2(a) and 2(c)]. As $\lambda_{\text{add}}/(\lambda_{\text{add}} + \lambda_{\text{remove}})$ increases beyond this low-connectivity regime, node connections are decreased by limiting node degree to a maximum of two, reducing effective diffusivity and increasing MFPT in these networks compared to networks without this constraint. As $\lambda_{\text{add}}/(\lambda_{\text{add}} + \lambda_{\text{remove}})$ exceeds approximately 0.7, further increase in $\lambda_{\text{add}}/(\lambda_{\text{add}} + \lambda_{\text{remove}})$ decreases effective diffusivity and increases MFPT if node degree is restricted to a maximum of two because the network freezes into linear or looped fragments.

To identify different particle spread regimes, we show in Figs. 2(e) and 2(f) the effective diffusivity and MFPT as the ratio of fusion (node connection) and fission (disconnection) rates $\lambda_{\text{add}}/\lambda_{\text{remove}}$ is varied. For sufficiently low $\lambda_{\text{add}}/\lambda_{\text{remove}}$ the effective diffusivity [Fig. 2(e)] for all networks is proportional to $\lambda_{\text{add}}/\lambda_{\text{remove}}$ because particle spread is limited by the probability that a particle can cross a newly formed fusion connection before the connection is removed (connection lifetime $= 1/\lambda_{\text{remove}}$), as well as the rate of connection formation ($\sim\lambda_{\text{add}}$). Similarly, for sufficiently low $\lambda_{\text{add}}/\lambda_{\text{remove}}$ the MFPT [Fig. 2(f)] decreases proportional to $\lambda_{\text{remove}}/\lambda_{\text{add}}$.

If $\lambda_{\text{remove}} \simeq 1$ for $\lambda_{\text{add}}/\lambda_{\text{remove}} < 1$, then D_{eff} falls below and MFPT increases above the low $\lambda_{\text{add}}/\lambda_{\text{remove}}$ trend at $\lambda_{\text{remove}} \simeq 1$ [Figs. 2(e) and 2(f)]. This is because particle motion across a connection is no longer limited by competition with connection lifetime ($\lambda_{\text{remove}} \lesssim 1$) but the network remains relatively disconnected ($\lambda_{\text{add}}/\lambda_{\text{remove}} < 1$). Particle spread thus falls below the low $\lambda_{\text{add}}/\lambda_{\text{remove}}$ trend, slowly increasing with the connectivity until the network becomes much more connected for $\lambda_{\text{add}}/\lambda_{\text{remove}} \simeq 1$. At $\lambda_{\text{add}}/\lambda_{\text{remove}} \simeq 1$ on degree-four networks the effective diffusivity rises to its maximum and MFPT falls to its minimum, remaining unchanged for further increased $\lambda_{\text{add}}/\lambda_{\text{remove}}$. If $\lambda_{\text{remove}} \simeq 1$ at $\lambda_{\text{add}}/\lambda_{\text{remove}} > 1$, then the transition from the low $\lambda_{\text{add}}/\lambda_{\text{remove}}$ trend is directly to the maximum D_{eff} and minimum MFPT [Figs. 2(e) and 2(f)].

On degree-two networks with fast dynamics (high λ_{add}) D_{eff} increases to a maximum for $\lambda_{\text{add}}/\lambda_{\text{remove}} \simeq 1$ as the network becomes more connected, before D_{eff} decreases at higher $\lambda_{\text{add}}/\lambda_{\text{remove}}$ as the network becomes maximally connected and freezes into linear or looped fragments [Figs. 2(e) and 2(f)]. On degree-two networks with slow dynamics (low λ_{add}) D_{eff} does not have an intermediate maximum at $\lambda_{\text{add}}/\lambda_{\text{remove}} \simeq 1$, instead increasing to a maximum D_{eff}. Similarly, on degree-two networks with fast dynamics MFPT decreases to a minimum for $\lambda_{\text{add}}/\lambda_{\text{remove}} \simeq 1$ and MFPT increases for higher $\lambda_{\text{add}}/\lambda_{\text{remove}}$ as the network freezes into linear or looped fragments.

Figure 3(a) shows the degree distribution as $\lambda_{\text{add}}/(\lambda_{\text{add}} + \lambda_{\text{remove}})$ is varied for both degree-4 and maximum degree-2 networks. At low $\lambda_{\text{add}}/(\lambda_{\text{add}} + \lambda_{\text{remove}}) \lesssim 0.2$, there are very few degree-3 and degree-4 nodes in the degree-4 networks, aligning with the similar D_{eff} and MFPT for degree-4 and maximum degree-2 networks in this connectivity range [Figs. 2(c) and 2(d)]. For $\lambda_{\text{add}}/(\lambda_{\text{add}} + \lambda_{\text{remove}}) \gtrsim 0.2$ the degree-3 and degree-4 nodes substantially rise for degree-4 networks [Fig. 3(a)], with this increasing difference from the maximum degree-2 network degree distribution consistent with the slower increase of D_{eff} and decrease of MFPT with increasing $\lambda_{\text{add}}/(\lambda_{\text{add}} + \lambda_{\text{remove}})$ for maximum

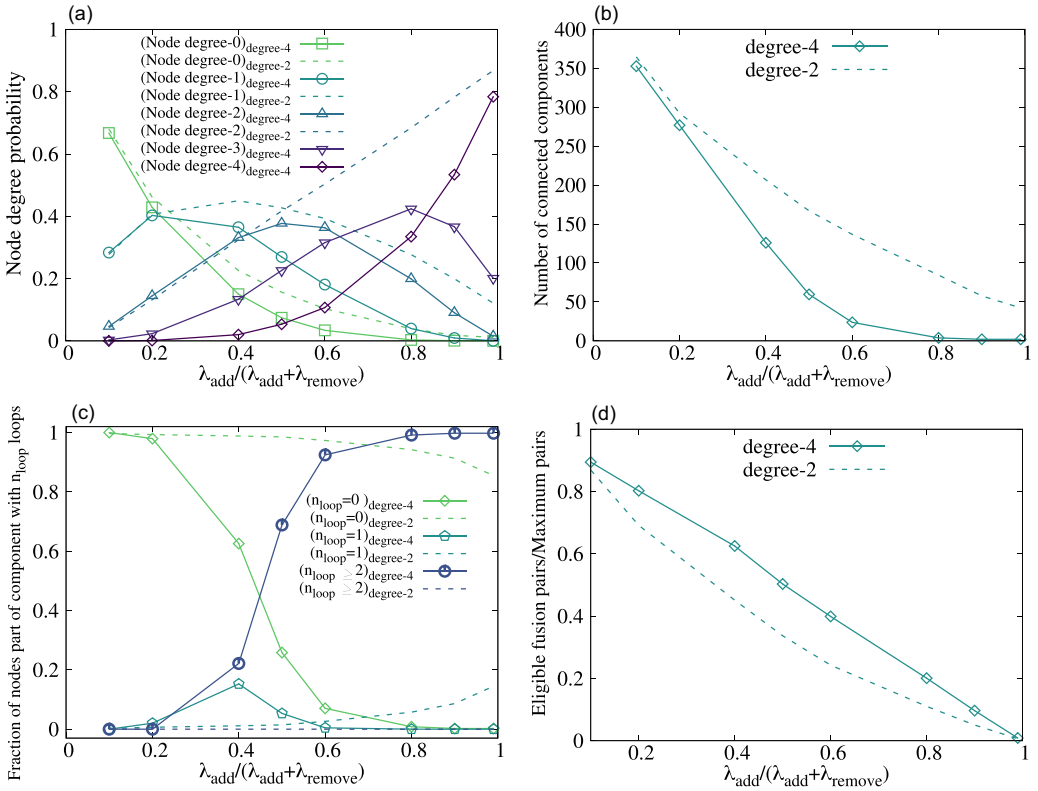

FIG. 3. Network structure and fusion capacity for model dynamic mitochondrial networks on a two-dimensional lattice. Across all panels, solid curves are degree-4 networks and dashed curves are maximum degree-2 networks. (a) Node degree distribution is compared for a degree-4 node and maximum degree-2 node mitochondrial network as fusion fraction of dynamics $\lambda_{add}/(\lambda_{add}+\lambda_{remove})$ is varied. Node degree indicated by legend. (b) The number of connected components as $\lambda_{add}/(\lambda_{add}+\lambda_{remove})$ is varied. (c) Fraction of nodes that are part of a connected component of a certain loop number (indicated by legend) as $\lambda_{add}/(\lambda_{add}+\lambda_{remove})$ is varied. Loop number is as previously defined for mitochondrial networks [9,10]. (d) The number of eligible fusion pairs as $\lambda_{add}/(\lambda_{add}+\lambda_{remove})$ is varied. The eligible fusion pairs is normalized by the maximum number of pairs, corresponding to a fully connected lattice. Across all panels, the lattice is 21×21 with nodes on a square grid with intervals of one, with quantities averaged over 10 sample networks. All panels are independent of network dynamics timescale τ.

degree-2 networks in this range, compared to degree-4 networks [Figs. 2(c) and 2(d)].

The linear and looped fragments in maximum degree-2 networks at high $\lambda_{add}/(\lambda_{add}+\lambda_{remove})$ can be seen in the right network inset of Fig. 2(c), as well as in the number of connected components and loop number of components in Figs. 3(b)–3(d). The large number of network components in Fig. 3(b) shows that at low $\lambda_{add}/(\lambda_{add}+\lambda_{remove})$ both degree-four and maximum degree-two networks are largely disconnected, consistent with similar D_{eff} and MFPT for the two network types. Although high $\lambda_{add}/(\lambda_{add}+\lambda_{remove})$ reduces the number of components to approach one for degree-four networks, for maximum degree-two networks the number of components remains far above one [Fig. 3(b)]. These degree-two networks, unable to branch, exhibit primarily linear components with some single-loop components [$n_{loop}=0$ and $n_{loop}=1$ dashed lines, respectively, in Fig. 3(c)] at high $\lambda_{add}/(\lambda_{add}+\lambda_{remove})$, while nodes for degree-four networks are nearly entirely in multiloop components [solid lines, Fig. 3(c)]. Figure 3(d) shows that for high $\lambda_{add}/(\lambda_{add}+\lambda_{remove})$ the number of eligible fusion connections for degree-two networks (only counting eligible connections to nodes with degree less than two) is even lower than the small number of eligible connections for the well-connected degree-four networks. Degree-two networks at high $\lambda_{add}/(\lambda_{add}+\lambda_{remove})$ are part of small linear and looped components, with few fusion opportunities.

For maximum degree-two networks, nodes that already have two connections to neighboring nodes cannot add a third connection, causing the formation of new connections to be coupled to the preceding removal of existing connections. At a fixed timescale of network dynamics $\tau = 1/(\lambda_{add}+\lambda_{remove})$, increasing $\lambda_{add}/(\lambda_{add}+\lambda_{remove})$ reduces λ_{remove}, slowing the rearrangement of the network. Particle confinement to a particular linear or looped fragment until the local network rearranges manifests as decreased diffusivity and increased MFPT compared to a less connected network with more rapid rearrangement dynamics. There is a smaller difference between degree-four and maximum degree-two networks for smaller τ (faster network dynamics) because the particles are confined to linear or looped fragments for shorter time periods.

Particles on degree-four dynamic lattice networks are found to monotonically increase their effective diffusivity and decrease their search time as connectivity increases. In contrast, networks limited to a maximum node degree of two

can see particles maximize effective diffusivity and minimize search time at intermediate connectivity, as the highest connectivity levels freeze linear and looped structures that decrease diffusivity and increase search time. The highest effective diffusivity and lowest search times on networks with a maximum node degree of two, which nearly match the maximum effective diffusivity and minimum search times on degree-four networks, are achieved for fast network rearrangement. Stated another way, while the maximum effective diffusivity and minimum search time on degree-four networks only modestly outperform those on networks limiting node degree to two, the degree-four networks can achieve this high performance with substantially slower network rearrangement dynamics.

These simulations vary network dynamics timescales relative to the fixed particle motion timescale. A high τ can represent any scenario with particle diffusion that is faster than network dynamics, such as a scenario with a rapidly diffusing ion in the mitochondrial matrix. A low τ can represent any scenario with diffusion that is much slower than network dynamics, such as a slowly diffusing membrane-embedded complex [55].

Thus far, the two-dimensional lattice-based model has considered a fixed lattice in a region of fixed size with varying connectivity between nearest-neighbor lattice sites. If lattice sites and connections both represent mitochondrial mass, then more connected networks have a higher total mitochondrial mass. Accordingly, we also considered the case of a fixed total mitochondrial mass, such that as the connectivity increases the lattice spacing increases. The resulting effective diffusivity and MFPT, shown in Fig. 10 in the Appendix, do not exhibit qualitative changes compared to the effective diffusivity and MFPT in Fig. 2. Although the distribution and connectivity of mitochondria in a cell may represent a tradeoff, these results suggest that this tradeoff may not qualitatively impact the spread through mitochondrial networks for mitochondria that are uniformly distributed in the cell.

B. Aspatial agent-based model

We now apply an existing aspatial mitochondrial network model [8] (see Fig. 1, right panel) in which each of N_{mito} minimal mitochondrial fragments do not have spatial positions and are represented by two permanently joined nodes. This mitochondrial network model is composed of three different node types: free nodes (degree-one nodes), degree-two nodes, and branching nodes (degree-three nodes). Two degree-one nodes can fuse with rate a_1 to form a connected degree-two node, lengthening a mitochondrial tube; and a degree-two node can fission into two degree-one nodes with rate b_1. A free node can undergo end-to-side fusion with a degree-two node with rate a_2 to form a degree-three node, branching a mitochondrial tube; and a degree-three node can fission into a degree-two node and a free node with rate b_2. Nodes may not fuse to their permanently connected partner node. A particle on a particular minimal mitochondrial fragment can move to any connected mitochondrial fragment (randomly selected if more than one other fragment is connected) with a rate of $k_m = 1$, setting the timescale. Model dynamics and particle motion are simulated using the Gillespie algorithm [53].

This representation of a mitochondrial network allows the network to be fragmented into many components or well connected into primarily larger components as fusion and fission rates are varied. This model also provides the observed network structure of mitochondria, includes branches, and assumes the network components are well-mixed in the cell volume [8].

Figure 4(a) shows the MFPT for a particle initially on a randomly selected minimal mitochondrial fragment to find another randomly selected target fragment as the ratio of end-to-end fusion to fission, $a_1 N_{\text{mito}}/b_1$, is varied. This ratio is analogous to the $\lambda_{\text{add}}/\lambda_{\text{remove}}$ varied in Figs. 2(e) and 2(f) for lattice networks. For both degree-three model mitochondrial networks that permit branching [$a_2 \neq 0$, solid curves in Fig. 4(a)] and degree-two networks that do not permit branching [$a_2 = 0$, dashed curves in Fig. 4(a)], for highly fragmented networks with low $a_1 N_{\text{mito}}/b_1$ the MFPT is proportional to $b_1/(a_1 N_{\text{mito}})$. This trend is due to particle motion that is limited by the probability that a particle in one mitochondria crosses a newly formed but short-lived fusion connection to another mitochondria, similar to the MFPT $\sim\lambda_{\text{remove}}/\lambda_{\text{add}}$ trend in Fig. 2(f).

For branching mitochondrial networks [solid curves in Fig. 4(a)], the MFPT stops decreasing along the $\sim b_1/(a_1 N_{\text{mito}})$ trend for all end-to-end fusion a_1 rates at $a_1 N_{\text{mito}}/b_1 \simeq 0.1$–$1$. This change in the MFPT trend is because the search time on the decreasing trend is approaching the minimum search time.

The minimum search time corresponds to the scenario that a particle will diffuse to a randomly selected mitochondrial fragment as quickly as the particle can diffuse from one mitochondrial fragment to another. The mean time to find a target mitochondrial fragment is the product of the time per attempt (diffusion to another mitochondrial fragment) and the mean number of attempts necessary to find the target fragment, $\langle T_{\text{min}}\rangle = \tau_{\text{attempt}}\langle N_{\text{attempts}}\rangle$, with $\tau_{\text{attempt}} = 1/k_m$. With the probability $1/N_{\text{mito}}$ that each successive attempt is successful and the probability $[(N_{\text{mito}}-1)/N_{\text{mito}}]^{n-1}$ that the first $n-1$ attempts are unsuccessful, the probability that the target fragment will be found on attempt n is

$$P(n) = \frac{1}{N_{\text{mito}}}\left(\frac{N_{\text{mito}}-1}{N_{\text{mito}}}\right)^{n-1}. \tag{1}$$

With the mean number of attempts $\langle N_{\text{attempts}}\rangle = \sum_{n=0}^{\infty} nP(n)$, then

$$\langle T_{\text{min}}\rangle = \frac{1}{k_m}\sum_{n=1}^{\infty}\frac{n}{N_{\text{mito}}}\left(\frac{N_{\text{mito}}-1}{N_{\text{mito}}}\right)^{n-1}, \tag{2}$$

$$\langle T_{\text{min}}\rangle = \frac{1}{k_m(N_{\text{mito}}-1)}\sum_{n=1}^{\infty} n\left(\frac{N_{\text{mito}}-1}{N_{\text{mito}}}\right)^{n}, \tag{3}$$

$$\langle T_{\text{min}}\rangle = \frac{N_{\text{mito}}}{k_m}, \tag{4}$$

with the final line applying $\sum_{n=1}^{\infty} nx^n = x/(x-1)^2$ for $x < 1$. Thus, the minimum search time is the product of the number of mitochondrial fragments and the timescale for particle diffusion between fragments.

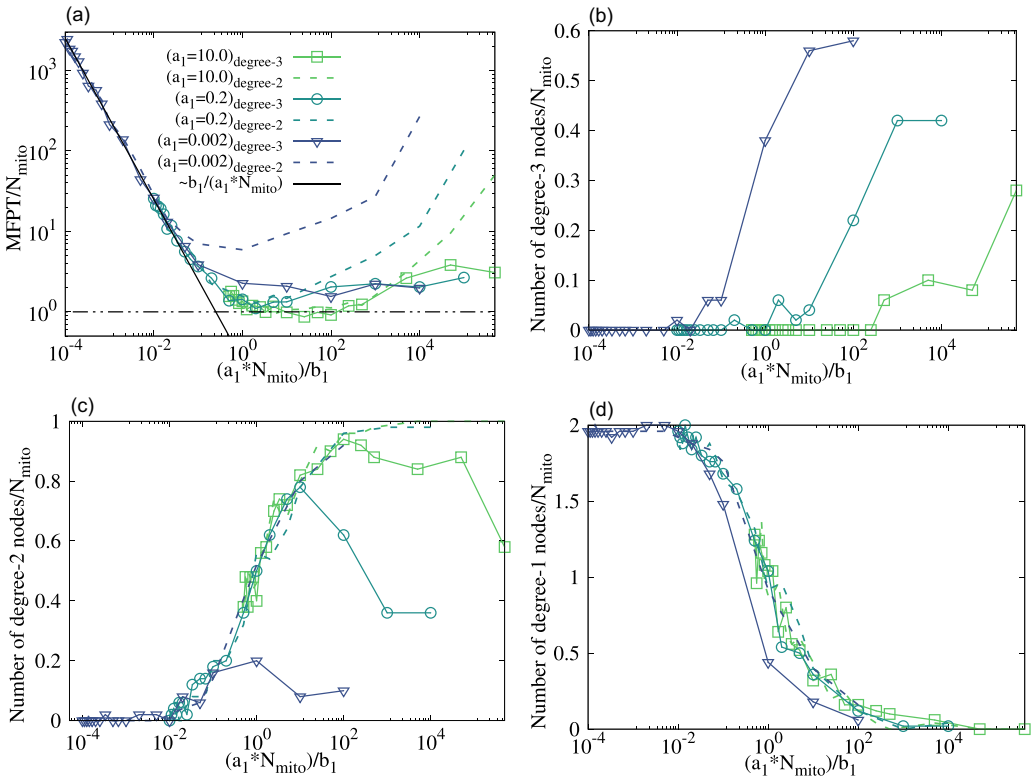

FIG. 4. Search times for particle diffusing on and node degree distribution of model aspatial dynamic mitochondrial networks. For all panels, solid curves are for branching (degree 3, end-to-side fusion rate $a_2 = 0.01$) networks, and dashed curves are nonbranching (degree 2, $a_2 = 0$) networks. (a) MFPT of a particle to find a randomly selected mitochondrial fragment from an initial location on another randomly selected fragment, as the scaled ratio of end-to-end fusion to fission $a_1 N_{\text{mito}}/b_1$ is varied. Solid black line is MFPT $\sim b_1/(a_1 N_{\text{mito}})$ trend and dot-dashed black line is minimum search time $\langle T_{\text{min}} \rangle$ from Eq. (4). Legend for (a) indicates end-to-end fusion rate a_1 and further applies to (b)–(d). (b–d) The scaled number of (b) three-way junctions (degree-three nodes), (c) end-to-end fusions (degree-two nodes), and (d) free ends (degree-one nodes) as $a_1 N_{\text{mito}}/b_1$ is varied, with network branching via end-to-side fusion. Across all panels, the end-to-side fusion rate for branching (degree-3) networks is $a_2 = 0.01$, the rate to move to connected mitochondrial fragments is $k_m = 1$, the number of minimal mitochondrial fragments $N_{\text{mito}} = 50$, and data averaged over 100 samples.

For $a_1 N_{\text{mito}}/b_1 \gtrsim 1$ the MFPT for branching networks [solid curves in Fig. 4(a)] is mostly independent of $a_1 N_{\text{mito}}/b_1$, with approximately flat MFPT in Fig. 4(a), because in this regime the networks are well connected with frequent end-to-end and/or many end-to-side connections, facilitating rapid search. Solid curves in Fig. 4(c) show the number of degree-two nodes for branching networks rises above zero at $a_1 N_{\text{mito}}/b_1 \simeq 10^{-2}$–$10^{-1}$. For rapid end-to-end fusion (high a_1) the number of degree-two nodes continues to rise as $a_1 N_{\text{mito}}/b_1$ further increases, while for slower fusion (low a_1) the number of degree-two nodes only rises somewhat before decreasing.

Degree-two nodes can undergo end-to-side fusion with a free end (degree-one node) to become a branch in the mitochondrial network (degree-three node). As shown in Fig. 4(b), the value of $a_1 N_{\text{mito}}/b_1$ above which degree-three nodes increase depends on the end-to-end fusion rate a_1, with degree-three nodes increasing at the $a_1 N_{\text{mito}}/b_1$ value at which degree-two nodes (solid curves) decrease in Fig. 4(c), indicating that the increase in degree-two nodes is converted to an increase in degree-three nodes. The $a_1 N_{\text{mito}}/b_1$ value for a branched network at which degree-two nodes decrease and degree-three nodes increase depends on the end-to-end fusion rate a_1 because fusion of a degree-two node and a free end to form a degree-three node competes with fission into two free ends. The initial rise in degree-two nodes for a branched network at $a_1 N_{\text{mito}}/b_1 \simeq 10^{-2}$–$10^{-1}$ is because this combination represents the balance between end-to-end fusion and fission. However, the balance between a degree-two node either fusing with a free end to form a degree-three node at rate a_2 or undergoing fission to form two free ends at rate b_1 is controlled by the ratio of a_2/b_1—at a given $a_1 N_{\text{mito}}/b_1$ in Figs. 4(b) and 4(c) a higher end-to-end fusion rate a_1 defines a higher b_1, such that increasing the number of degree-three nodes requires more degree-two nodes, which occurs at higher $a_1 N_{\text{mito}}/b_1$. We see corresponding changes in the number of free ends (degree-one nodes) in solid curves of Fig. 4(d), as the number of free ends decreases when degree-two nodes increase in Fig. 4(c) (solid curves). Recent modeling work shows similar trends in the number of degree-three, degree-two, and degree-one nodes as the ratio of fusion to fission is varied [19].

For nonbranching networks [dashed curves in Fig. 4(a)], the MFPT stops decreasing along the $\sim b_1/(a_1 N_{\text{mito}})$ trend when $b_1 \simeq 1$. For low $a_1 \lesssim 0.1$, as $a_1 N_{\text{mito}}/b_1$ increases above the value at which $b_1 \simeq 1$, the MFPT is controlled by the timescale of mitochondrial dynamics, with particles waiting for new connections to search for the target mitochondrial

fragment, and increasing a_1 leads to lower MFPT. For higher $a_1 \gtrsim 0.1$, as $a_1 N_{\text{mito}}/b_1$ increases above $b_1 \simeq 1$, the MFPT is controlled by the timescale of particle motion, with many connections allowing the particle to continuously diffuse to another mitochondrial fragment as it undergoes a search for the target mitochondrial fragment. This corresponds to the minimum search time $\langle T_{\text{min}} \rangle$ of Eq. (4). At sufficiently high $a_1 N_{\text{mito}}/b_1 \gtrsim 10^2$, the MFPT for nonbranching networks increases [dashed curves in Fig. 4(a)]. This is distinct behavior in comparison to branching networks, which have a flat MFPT independent of fission and fusion rates for high $a_1 N_{\text{mito}}/b_1$. This increasing MFPT for nonbranching networks is because the network freezes into linear and looped fragments as the fission rate b_1 becomes low, and the number of free ends (degree-one nodes) decreases to nearly zero [dashed curves in Fig. 4(d)] and nearly all nodes are part of end-to-end fusions [degree-two nodes, dashed curves in Fig. 4(c)] for $a_1 N_{\text{mito}}/b_1 \gtrsim 10^2$. Although the degree-two and degree-one node populations for branched networks [solid curves in Figs. 4(c) and 4(d), respectively] change as a_1 is varied, without branching the degree-two and degree-one node populations [dashed curves in Figs. 4(c) and 4(d), respectively] are independent of a_1 and are determined by $a_1 N_{\text{mito}}/b_1$ as these nonbranched networks are only balancing end-to-end fusion and fission.

The freezing of the nonbranching networks into linear and looped fragments for low b_1 is shown in Figs. 5(a) and 5(b), which show branched and unbranched sample network structures at low and high connectivity. Branching and nonbranching networks both similarly decrease the number of connected components as $a_1 N_{\text{mito}}/b_1$ rises [Fig. 5(c)]; this is distinct from the number of components for lattice networks in Fig. 3(b) because nonbranching aspatial networks are not restricted to fusing to their neighbors. As $a_1 N_{\text{mito}}/b_1$ increases, the branching networks switch from linear components [Fig. 5(d)] to single-loop components [Fig. 5(e), main plot] to multiloop components [Fig. 5(e), inset]. In contrast, nonbranching networks switch from linear to single-loop components at higher $a_1 N_{\text{mito}}/b_1$ values [Figs. 5(d) and 5(e)], as the formation of single loops requires two free ends for nonbranching networks. For both branching and nonbranching networks the number of eligible fusion pairs becomes small as the fusion rate increases [Fig. 5(f)]. Nonbranching networks at high $a_1 N_{\text{mito}}/b_1$ are part of large linear and single-looped components, with few fusion opportunities.

Particles on both branching and nonbranching model aspatial mitochondrial networks decrease their search time as the networks increase their connectivity from nearly entirely fragmented to well-connected networks. Once a branching network has become well connected, further increases in fusion, decreases in fission, or changes to the timescale of network dynamics have a limited effect on search time. In contrast, once a nonbranching network has become well connected if fusion is sufficiently increased or fission sufficiently decreased, then MFPT substantially rises as the network becomes frozen into looped and linear fragments. For nonbranching networks, the timescale of network dynamics affects the minimum MFPT reached, with fast dynamics achieving lower MFPT than slow dynamics. Nonbranched networks with sufficiently fast dynamics are also able to achieve the minimum MFPT achieved by branched networks across timescales of dynamics. Overall, the minimum MFPT achieved by branching networks with all dynamical timescales can only be achieved by nonbranching networks with fast dynamics, with nonbranching networks with slow dynamics exhibiting substantially longer search times.

A single end-to-side fusion rate a_2 is insufficient to explore the range of possible mitochondrial network connectivity, as the levels of free ends (degree-one nodes), end-to-end fusions (degree-two nodes), and end-to-side fusions (degree-three nodes) depend nonlinearly on the fusion-fission ratios a_1/b_1 and a_2/b_2 [8]. In our simulations of aspatial mitochondrial networks with branching thus far, the end-to-side fusion rate is set to $a_2 = 0.01$ (Fig. 4). This a_2 value is selected to provide an intermediate level of network branching, with similar a_2 values (increased or decreased by an order of magnitude) similarly providing an MFPT $\sim b_1/(a_1 N_{\text{mito}})$ trend for fragmented networks at low $a_1 N_{\text{mito}}/b_1$ and an unchanging MFPT for well-connected networks at higher $a_1 N_{\text{mito}}/b_1$, as shown in Fig. 4(a) (solid curves) and the Appendix Figs. 11(b) and 11(c). A substantially decreased a_2 value provides less branching and leads toward the MFPT behavior for unbranched networks, with lower end-to-side fusion causing longer MFPT at a given $a_1 N_{\text{mito}}/b_1$ [Fig. 4(a), dashed curves, and the Appendix Fig. 11(d)]. A substantially increased a_2 value provides denser branching and leads to MFPTs that are shorter than the $\sim b_1/(a_1 N_{\text{mito}})$ trend [Appendix Fig. 11(a)] in the nearly disconnected network regime, with branching connecting short mitochondria with end-to-side fusions to other mitochondria, enabling a particle to more rapidly sample more mitochondria.

These simulations vary network dynamics timescales relative to the fixed rate at which particles move to connected mitochondria fragments, $k_m = 1$, setting the timescale. Across the a_1 range explored for branching networks with $a_2 = 0.01$ [solid curves, Fig. 4(a)], particle search is affected little by whether particle motion is relatively fast or slow. For the unbranched networks [dashed curves, Fig. 4(a)], particles with slower diffusion relative to the speed of network dynamics (large a_1) lead to lower MFPT, as the mitochondrial fragment has the opportunity to rearrange connections, which could represent a protein diffusing in a mitochondrial network with rapid dynamics or a slowly diffusing protein complex in a mitochondrial network with typical dynamics. Also, on unbranched networks, particles that are more diffusive relative to the speed of network dynamics (small a_1) could represent a protein diffusing in a mitochondrial network with slow dynamics or a rapidly diffusing ion in mitochondria with rapid dynamics. Figure 4 explored a mitochondrial network with $N_{\text{mito}} = 50$ minimal mitochondria fragments, with larger networks ($N_{\text{mito}} = 100$) showing very similar MFPTs (Appendix Fig. 12).

III. DISCUSSION

Mitochondria form dynamic tubular networks that continuously remodel their structure through fusion and fission processes. These dynamics are proposed to enable the sharing of mitochondrial proteins and other molecules, evening out heterogeneous delivery of nuclear-encoded proteins and com-

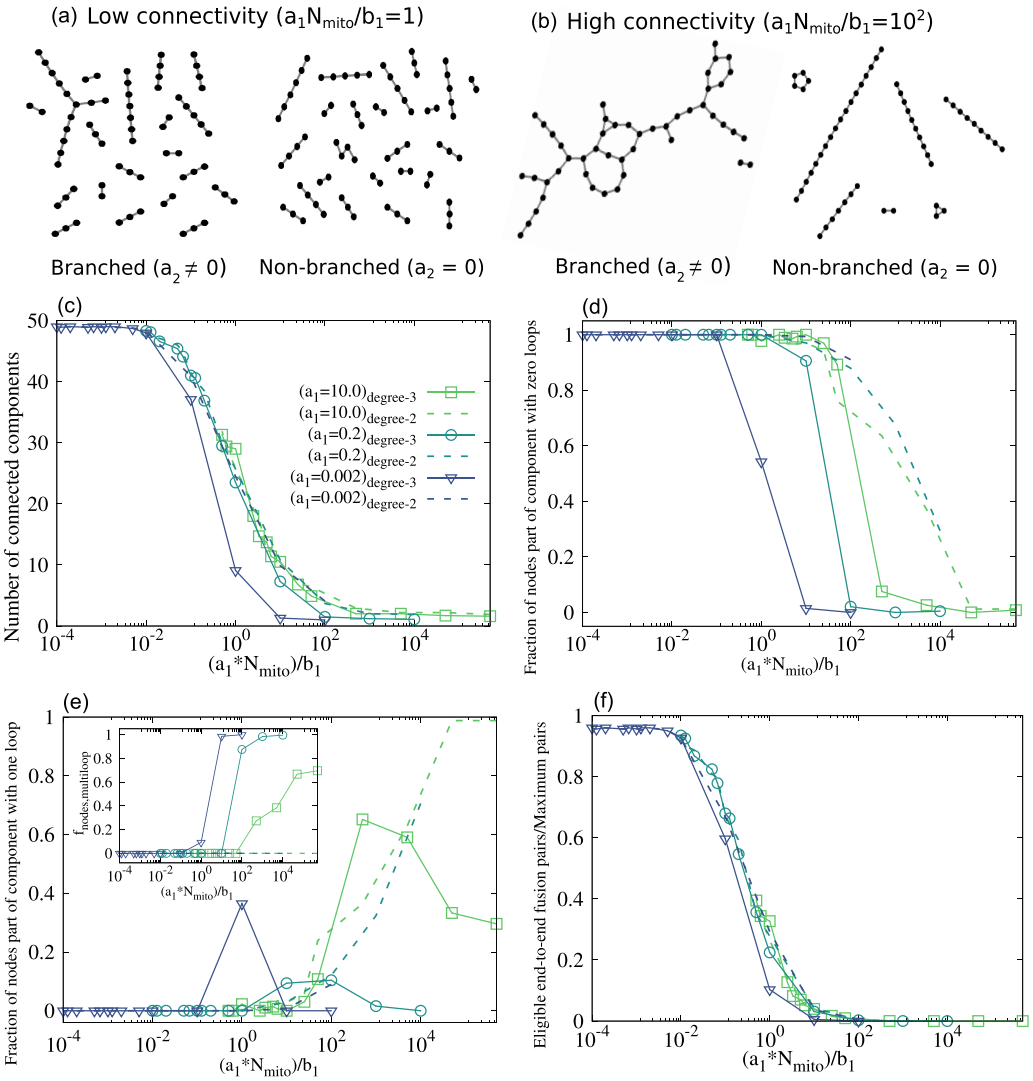

FIG. 5. Network structure and fusion capacity for model aspatial dynamic mitochondrial networks. (a and b) Sample network structures for branched ($a_2 \neq 0$) and nonbranched networks ($a_2 = 0$) for a (a) low-connectivity regime ($a_1N_{mito}/b_1 = 1$) and (b) high-connectivity regime ($a_1N_{mito}/b_1 = 10^2$). (c) The number of connected components as the scaled ratio of end-to-end fusion to fission a_1N_{mito}/b_1 is varied. Legend for (c) applies to (c)–(f) and indicates end-to-end fusion rate a_1 and whether the network permits branching (solid curves) and formation of degree-3 nodes (degree 3) or does not permit branching (degree 2, dashed curves). (d and e) Fraction of nodes that are part of a connected component with (d) zero loops, (e) one loop, and (e, inset) two or more loops, as a_1N_{mito}/b_1 is varied. Note that the spike in the fraction of nodes on a component with one loop for $a_1 = 0.002$ degree-3 networks is caused by the transition from networks with primarily zero-loop to multiple loop components at $a_1N_{mito}/b_1 \simeq 1$. (f) Number of eligible end-to-end fusion pairs as a_1N_{mito}/b_1 is varied. Eligible end-to-end fusion pairs is normalized by the maximum number of pairs, which is for an entirely disconnected network. Across all panels, the end-to-side fusion rate for branching (degree-3) networks is $a_2 = 0.01$ and for nonbranching (degree-2) networks is $a_2 = 0$, the number of minimal mitochondrial fragments is $N_{mito} = 50$, and quantities are averaged over ten sample networks.

plementing mutant protein copies from nearby mitochondrial DNA copies with those from more distant copies, among other advantages from sharing molecules [31,37,39]. Mitochondrial networks can range from fragmented [18] to highly connected structures [9,43], depending on the cell type and environment. We build on previous quantitative modeling of mitochondrial network dynamics, using a two-dimensional spatial lattice [31] and an aspatial agent-based model [8], to explore how fusion and fission levels control the spread of particles through the mitochondrial network.

As expected, better-connected networks and networks with faster fusion and fission dynamics each lead to increased particle spread for both spatial and aspatial networks. For branching networks, once the mitochondrial network is sufficiently well connected, further increases in connectivity do not substantially increase particle spread. This is similar to a percolation transition in two dimensions [54], matching descriptions of mitochondrial networks as approaching effectively two dimensional [9,21,44].

For the most fragmented networks with much faster fission than fusion, particle spread is limited by the speed of fission dynamics as fission competes with the timescale for particle movement between fused mitochondria, with particle spread increasing as fission slows. If the network becomes

well connected while fission is still rapid compared to particle motion between mitochondria, then the increase in spread primarily occurs due to slowing fission competing less with but still limiting particle motion, and the network becoming well connected halts further improvement in spread. This scenario applies to particles with relatively low diffusivity within mitochondria, such as large membrane complexes. If the fission rate instead slows to no longer compete with particle motion (particles have plenty of time to cross a recently formed fusion connection), then on the spatial lattice-based network spread will plateau until fisson decreases sufficiently that the network becomes well connected, causing particle spread to become more rapid and reach a maximum. On the aspatial network, the particles instead never reach the fastest spread. This distinction is because on the spatial network, more connectivity always benefits spread even if network dynamics are slow, while on the aspatial network high connectivity combined with slow dynamics can lead to persistent disconnected subnetworks. This scenario, of particles easily crossing a fusion connection before fission removes the connection, applies to particles with relatively high diffusivity within mitochondria, such as ions or soluble proteins in the mitochondrial matrix.

Experimental measurements of protein spread on mitochondrial networks support these two regimes of particle spread, one regime limited by fission events occurring before particles can cross the fused connection and the other regime defined by fusion event lifetimes much longer than the timescale for particles to cross the fused connection. While fusion events with long lifetimes enable ongoing protein spread, short-lived mitochondrial "kiss-and-run" fusion events also allow substantial exchange of soluble proteins but limited exchange of membrane proteins between mitochondrial fragments [56], and can enable meaningful protein delivery for extended mitochondrial networks [57]. Soluble proteins are also observed to spread through yeast mitochondrial networks in minutes following fusion, while protein components of the oxidative phosphorylation machinery, which form membrane-embedded complexes and can be largely confined to cristae, show limited spread through the network more than an hour after fusion [58]. Beyond molecule size and membrane embedding, which can influence diffusivity in mitochondria, various protein-specific and environmental variables influence diffusivity patterns [59].

An important mitochondrial network feature is their three-way junctions, formed via end-to-side fusion, as they enable branching and looping of mitochondrial networks [9–11]. Our model explores both branching model mitochondrial networks with three-way junction formation and nonbranching networks that are not permitted to form three-way junctions. Particle spread on branching model mitochondrial networks (described above) is modified for nonbranching networks. Diffusive particles on both branching and nonbranching networks can achieve comparably fast spread, however, nonbranching networks require much faster fusion and fission dynamics to achieve the most rapid spread. This suggests that one advantage of branching mitochondrial networks is to enable the efficient spread of proteins and other molecules with much lower costs associated with the very rapid fusion and fission that would be necessary for efficient spread in a nonbranching mitochondrial network. Furthermore, spread on nonbranching mitochondrial networks does not remain maximized once networks are sufficiently well connected. Instead, nonbranching networks have an optimum connectivity that maximizes spread, with both lower and higher connectivity decreasing spread. While less spread for less connectivity is similar to branching networks, more connectivity causes decreased spread on nonbranching networks because the network freezes into linear fragments and loops.

The mitochondria modeled as a spatial network on a two-dimensional lattice and as an aspatial agent-based network differ in how particle spread changes as fission slows compared to fusion (described above) and in how spread on nonbranching networks approaches spread on branching networks. For spatial networks, the particle spread timescale on nonbranching networks does not achieve the lower spread timescale of branching networks, while for aspatial networks the spread timescale on nonbranching networks (with fast dynamics and optimum connectivity) can reach the spread timescale on branching networks. This distinction, with spread on nonbranched spatial networks persistently disadvantaged relative to branched networks, demonstrates the important effect of embedding a network in physical space [60]. Rapid dynamics does not entirely rescue the slow spread on nonbranching spatial lattice-based mitochondrial networks because mitochondrial fragments embedded on a spatial lattice are constrained to connect to the same few nearby fragments. Very recent work developed a mitochondrial network model permitting mitochondrial fragment motion, integrating the spatial aspect of our lattice model with the changing fusion partners of our aspatial model [19]. Although that work did not examine particle spread, frequent network rearrangements were found to require intermediate fusion rates, to allow recently fissioned mitochondrial fragments to separate without refusing, suggesting the spatially embedded nature of mitochondria constrains network structure and downstream processes such as spread.

Yeast mitochondria are well connected into a small number of network components [9], while mammalian mitochondria can be near the percolation transition threshold with a range of fragment sizes [8,43]. We then expect that yeast are typically near optimized spread and a substantial shift toward fragmentation via more fission or less fusion would correspondingly slow spread through the mitochondrial network. Mammalian mitochondria are instead in the regime with spread affected by smaller changes to connectivity. However, mammalian mitochondria have relatively fast dynamics [19], such that for many proteins and other molecules spread may be limited by competition between intramitochondrial diffusion and fission, a regime that yields faster spread across parameter values. In contrast to both yeast and mammals, plant mitochondrial networks are very fragmented [23], suggesting spread through plant mitochondria is significantly hindered compared to better-connected networks and sensitive to the frequency and lifetime of fusion connections.

Previous modeling work has probed how mitochondrial network structure and dynamics impacts spread. For a static network, recent modeling work showed that mitochondrial network snapshots that contain loops allow faster diffusive search compared to networks without loops [9,10]. We similarly found that for dynamic mitochondrial networks, a

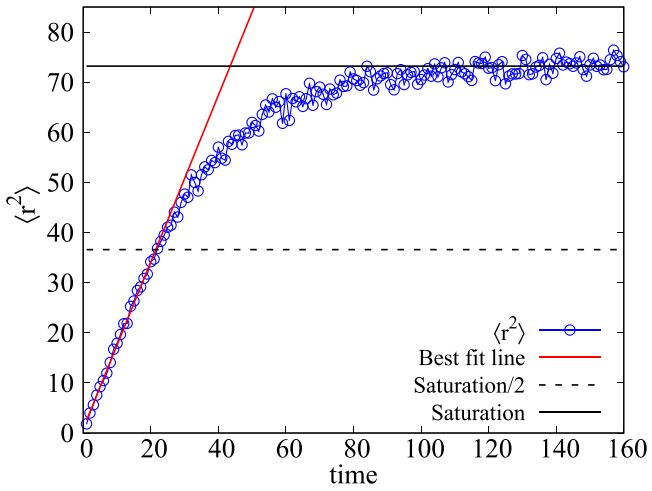

FIG. 6. Example D_{eff} calculation from mean squared displacement $\langle r^2(t)\rangle$ vs. time t. Blue circles are $\langle r^2(t)\rangle$ averaged over 100 samples. The solid red curve is the linear fit up to half of the $\langle r^2\rangle$ saturation value (half saturation indicated as dashed black line, saturation as solid black line).

larger number of loops facilitates faster spread. Our results in Fig. 2(a) recapitulated earlier mean-field calculations and stochastic simulations for spread on a two-dimensional lattice model of a mitochondrial network, which showed a stronger dependence of effective diffusivity on connectivity for slower dynamics [31]. A two-dimensional spatial model with mitochondrial motion along filaments suggested there may be a minimum mitochondrial fusion rate above which lack of exchange impacts mitochondrial health [21], and an aspatial mitochondrial model indicated more frequent fusion suppresses protein concentration fluctuations between mitochondria [37], aligning with our results that show changes in spread as the ratio of fusion to fission is varied, including relatively sudden changes in spread at particular ratios of fusion to fission for certain parameter values. A model of heavily fragmented mitochondria using a contact measure of spread suggested mitochondrial DNA gene products efficiently spread for parameters describing living plant cells, which are relatively fragmented [46], suggesting different measures of spread may be optimized for different network dynamics. Notably, little to no previous work addressed how spread is impacted by the end-to-side fusion processes that form branches in mitochondrial networks.

Beyond a specific focus on mitochondria, spread on dynamic and static networks has long been explored. Earlier work using mean-field techniques on fluctuating disordered lattices found transition rates dependent upon fluctuation timescale and bond probability [47,48,52], predicting the effective diffusivity of Fig. 2(a). Walkers that transition between nodes with non-Poisson time distributions have occupation probability distributions across node degree that are distinct on Erdős-Rényi versus Barabási-Albert networks [52], indicating steady-state walker distributions can be affected by network structure, and mean first-passage times that transition more suddenly with varying node-to-node transition rates [51], suggesting nontrivial interaction between the network fluctuations and walker transitions between nodes. Beyond dynamic networks, on percolating static networks with site probability p near the percolation threshold p_c, particles on static lattices exhibit effective diffusivity $D_{\text{eff}} \sim (p - p_c)^{\mu}$ with exponent $\mu \simeq 1.3$ for two-dimensional lattices [54]. On static complex networks, mean first-passage time depends on the degree of the target node, the connectivity of the network overall, and the motion characteristics of the searcher [61–63]. Thus, for spread on both dynamic and static networks the connectivity details and walker motion characteristics are important, and for dynamic networks rearrangement timescales also play a role, corresponding well with our finding that branching as well as the relative particle diffusion and network rearrangement timescales are important for spread on mitochondrial networks.

Through quantitative modeling of spread on mitochondrial networks, we have identified network branching at three-way junctions as crucial to allow efficient spread with relatively slow mitochondrial fusion and fission dynamics. We have also shown that spread falls into different regimes that correspond to regimes of network connectivity: on fragmented networks spread is slow and depends on marginal changes to fusion and fission, while on well-connected networks spread is rapid and

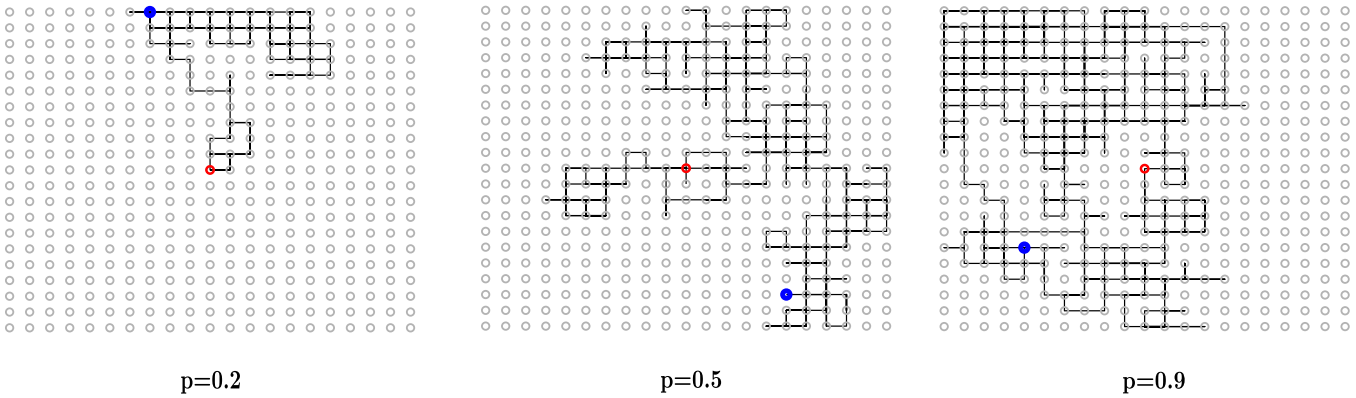

FIG. 7. Typical particle trajectories for different connection probabilities $p = 0.2$, $p = 0.5$, and $p = 0.9$ are shown over a simulation time of 10^3 for a degree-four network. Black solid lines represent the trajectory of the diffusing particle moving in a fluctuating network, with moves between lattice sites (gray open circles) only occurring when a connection is present. The particle starts at the red mark and finishes at the blue mark for each trajectory.

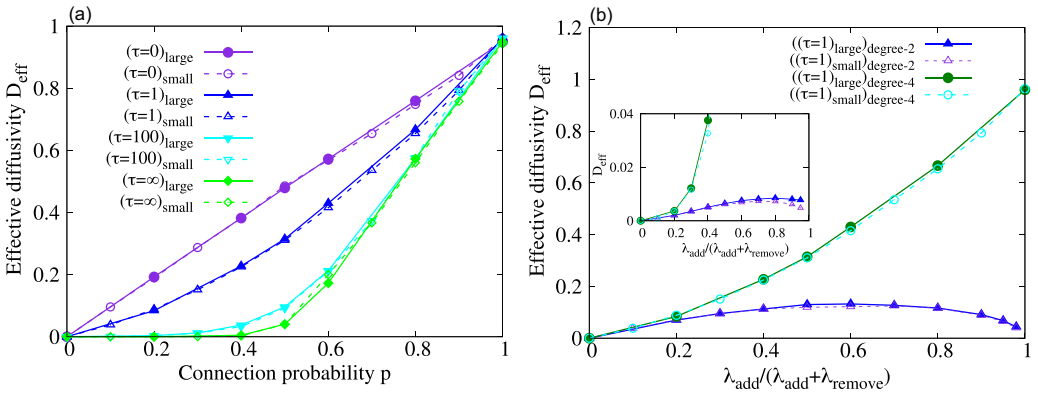

FIG. 8. Effective diffusivity D_{eff} for a different system size. (a) Effective diffusivity D_{eff} of a particle diffusing on the model dynamic mitochondrial network on a two-dimensional lattice as connection probability p is varied. Solid curves with filled markers are for a 41×41 lattice and dashed curves with open markers are for a 21×21 lattice, with nodes on a square grid with intervals of one. Legend indicates network dynamics timescale τ. (b) Effective diffusivity D_{eff} for particle diffusing on model dynamic mitochondrial network on two-dimensional lattice as fusion fraction of dynamics $\lambda_{\text{add}}/(\lambda_{\text{add}} + \lambda_{\text{remove}})$ is varied, for 21×21 (small, dashed curves) and 41×41 (large, solid curves) systems. Legend indicates system size and whether nodes can connect to all four nearest neighbors (degree 4) or only two nearest neighbors (degree 2). The main plot is for network dynamics timescale $\tau = 1$ and the inset is for $\tau = 100$. Legend applies to both the main plot and the inset. Particle diffusivity $D = 1$ and data averaged over 100 samples for both panels.

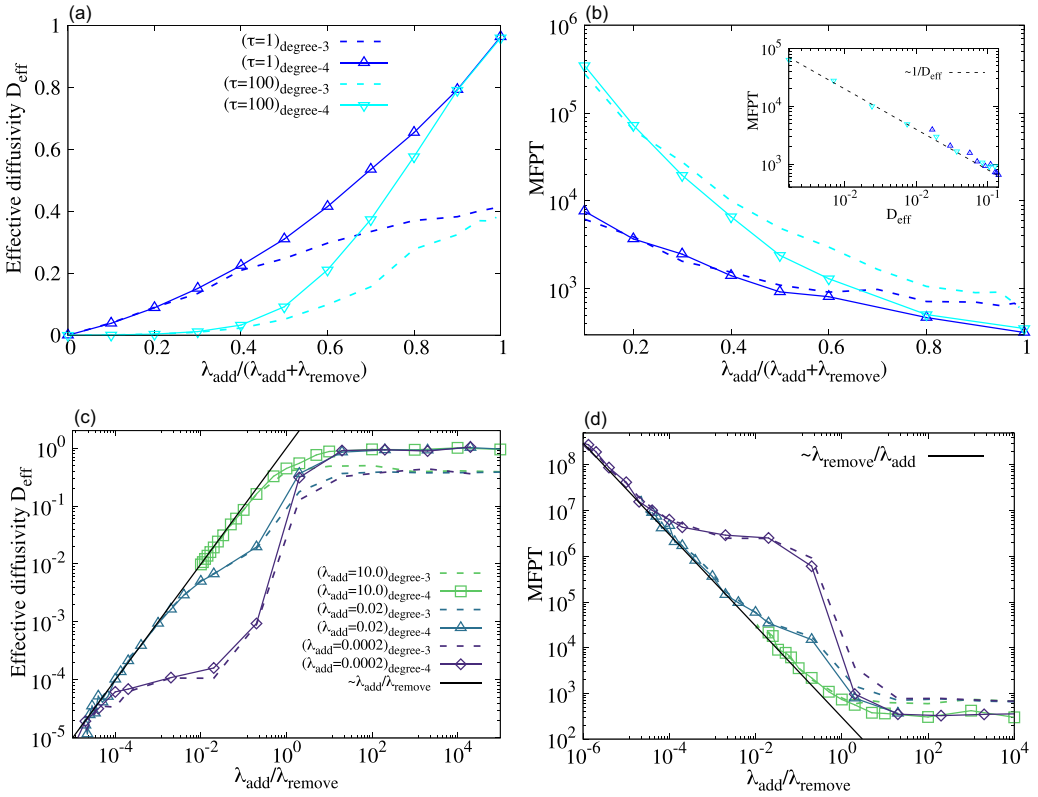

FIG. 9. Comparison of particle diffusivity and search time on lattice networks permitting degree-four and degree-three nodes. (a) Effective diffusivity D_{eff} as fusion fraction of dynamics $\lambda_{\text{add}}/(\lambda_{\text{add}} + \lambda_{\text{remove}})$ is varied. The legend in (a), which also applies to (b), indicates network dynamics timescale τ and whether nodes can connect to all four nearest neighbors (degree 4, solid curves) or only three nearest neighbors (degree 3, dashed curves). (b) MFPT as $\lambda_{\text{add}}/(\lambda_{\text{add}} + \lambda_{\text{remove}})$ is varied. Inset shows MFPT vs. D_{eff} from main plots of (a) and (b). Dashed black line in the inset shows $\sim 1/D_{\text{eff}}$ trend. (c) Effective diffusivity D_{eff} as balance between fusion and fission $\lambda_{\text{add}}/\lambda_{\text{remove}}$ is varied. Black line is $\sim\lambda_{\text{add}}/\lambda_{\text{remove}}$ trend. Legend entries for simulation data (those with λ_{add} values) in (c) also apply to (d). (d) MFPT as $\lambda_{\text{add}}/\lambda_{\text{remove}}$ is varied. Black line is $\sim\lambda_{\text{remove}}/\lambda_{\text{add}}$ trend. Across all panels, particle diffusivity $D = 1$, the lattice is 21×21 with nodes on a square grid with intervals of one, and data averaged over 100 samples.

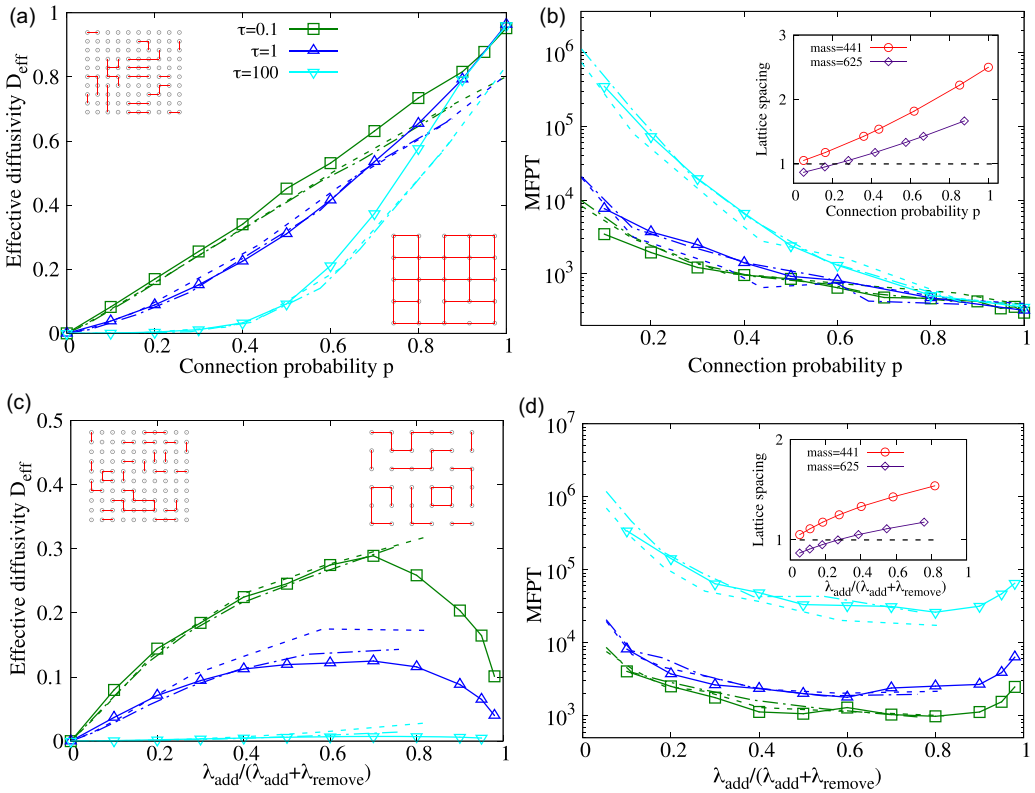

FIG. 10. Comparison of effective diffusivity D_{eff} and MFPT for the networks with varying and fixed total mitochondrial mass on a two-dimensional lattice. Across all panels, solid curves are for varying total mitochondrial mass (same as Fig. 2), dashed curves are for fixed total mitochondrial mass $m = 441$, dot-dashed curves are for mass $m = 625$, with particle diffusivity $D = 1$. (a) Effective diffusivity D_{eff} as the connection probability p is varied for degree-four networks. Insets show typical networks for $p = 0.16$ and $p = 0.85$ with $m = 441$. Legend in (a) indicates network dynamics timescale τ and also applies to (b)–(d). (b) The MFPT of a diffusing particle to find a randomly selected lattice site from initial position at another randomly selected lattice site, as connection probability p is varied for the degree-four network. Inset shows the lattice spacing for the fixed mass networks as connection probability p varies. (c) Effective diffusivity D_{eff} as fusion fraction of dynamics $\lambda_{\text{add}}/(\lambda_{\text{remove}} + \lambda_{\text{remove}})$ is varied for the degree-two networks. Insets show typical networks for $p = 0.16$ and $p = 0.45$ with $m = 441$. (d) MFPT as $\lambda_{\text{add}}/(\lambda_{\text{add}} + \lambda_{\text{remove}})$ is varied for the degree-two network. Inset shows the lattice spacing for the fixed mass networks as $\lambda_{\text{add}}/(\lambda_{\text{add}} + \lambda_{\text{remove}})$ is varied. Data averaged over 100 samples for all panels.

depends little on marginal changes to fusion and fission. By exploring both a spatial and aspatial model of mitochondrial dynamics, our results align with previous work suggesting that the spatial nature of mitochondria is important to network rearrangements. This work advances quantitative understanding of mitochondrial network structure and dynamics toward mechanistic connection to mitochondrial function.

Source code for simulations and analysis, and data for figures, is available from Ref. [64].

ACKNOWLEDGMENTS

A.I.B. acknowledges support from a Natural Sciences and Engineering Research Council of Canada (NSERC) Discovery Grant, by start-up funds provided by the Toronto Metropolitan University Faculty of Science, by the Toronto Metropolitan University Faculty of Science Dean's Research Fund, and computational resources provided by the Digital Research Alliance of Canada (alliancecan.ca), including those provided as part of a Resource Allocation cluster usage resource allocation. S.P.C. acknowledges support from an NSERC Discovery Grant.

APPENDIX: ADDITIONAL METHOD DETAILS AND RESULTS

1. Spatial lattice-based model

D_{eff} is calculated by fitting simulation data for mean squared displacement as a function of time $\langle r^2(t)\rangle$ to $\langle r^2\rangle = 4D_{\text{eff}}t$ to determine the slope $4D_{\text{eff}}$ and thus the effective diffusivity D_{eff}. The slope is fit up to half of the saturated $\langle r^2\rangle$ value due to the finite system size, with one example shown in Fig. 6.

Sample particle trajectories in the case of a degree-four network are shown in Fig. 7 for three different bond connection probabilities $p = 0.2$, $p = 0.5$, and $p = 0.9$.

The effective diffusivity D_{eff} versus connection probability p, as in Fig. 2(a) but for a larger system, is shown in Fig. 8(a). The larger system behaves nearly identically to the smaller network. Figure 8(b) similarly compares effective diffusivity for both degree-four and degree-two networks for a larger

system compared to the system for results in Fig. 2(c), finding the larger system behaves nearly identically to the smaller network.

Figure 9 compares effective diffusivity D_{eff} and MFPT of a particle on a dynamic spatial lattice network for the case with nodes only allowed to connect to three nearest neighbors (degree-three networks) to the case where nodes can connect to all four nearest neighbors [degree-four networks, Figs. 2(a) and 2(b)]. The qualitative D_{eff} and MFPT are unchanged, although D_{eff} substantially decreases and MFPT substantially increases at high $\lambda_{\text{add}}/(\lambda_{\text{add}} + \lambda_{\text{remove}})$ for degree-three networks compared to degree-four networks. This regime in which these networks differ is when the dynamics favor high connectivity, and thus the limit to three connections shows an effect.

In Fig. 2 we considered particle spread on the two-dimensional lattice-based model with a fixed lattice in a region of fixed size with varying connectivity between nearest-neighbor lattice sites. If lattice sites and connections both represent mitochondrial mass, then more connected networks have a higher total mitochondrial mass. Here, we consider the case of fixed total mitochondrial mass, such that as the connectivity increases the lattice spacing increases [compare inset networks of Fig. 10(a)]. We assume that each lattice site has a mitochondrial mass of one, that each fusion connection between nearest-neighbor lattice sites has a mass equal to its length (we do not vary this mass ratio but do not expect its variation to qualitatively affect our results), and that the time to cross a connection is proportional to its length squared.

There are n^2 lattice sites in an $n \times n$ lattice, and each fusion connection has a length $L/(n-1)$ with L the linear size of the system. The total mass m of an $n \times n$ lattice with a connection probability p is then

$$m = n^2 + 2nLp\,, \tag{A1}$$

which can be rearranged to find the connection probability

$$p = \frac{m - n^2}{2nL}\,. \tag{A2}$$

We fix the linear system size L and mass m, and then varying the number of sites n across the lattice controls the probability p.

We show effective diffusivity and MFPT for $L = 20$ (matching Fig. 2) and total masses $m = 441$ (matching Fig. 2 lattice spacing at $p = 0$) and $m = 625$ (matching Fig. 2 lattice spacing at $p \simeq 0.2$) in Figs. 10(a) and 10(b) for no limits on node degree. The effective diffusivity D_{eff} and MFPT are very similar to the networks that do not conserve mass in Fig. 2.

For networks with nodes limited to a maximum degree of two, we show the conserved-mass network results in

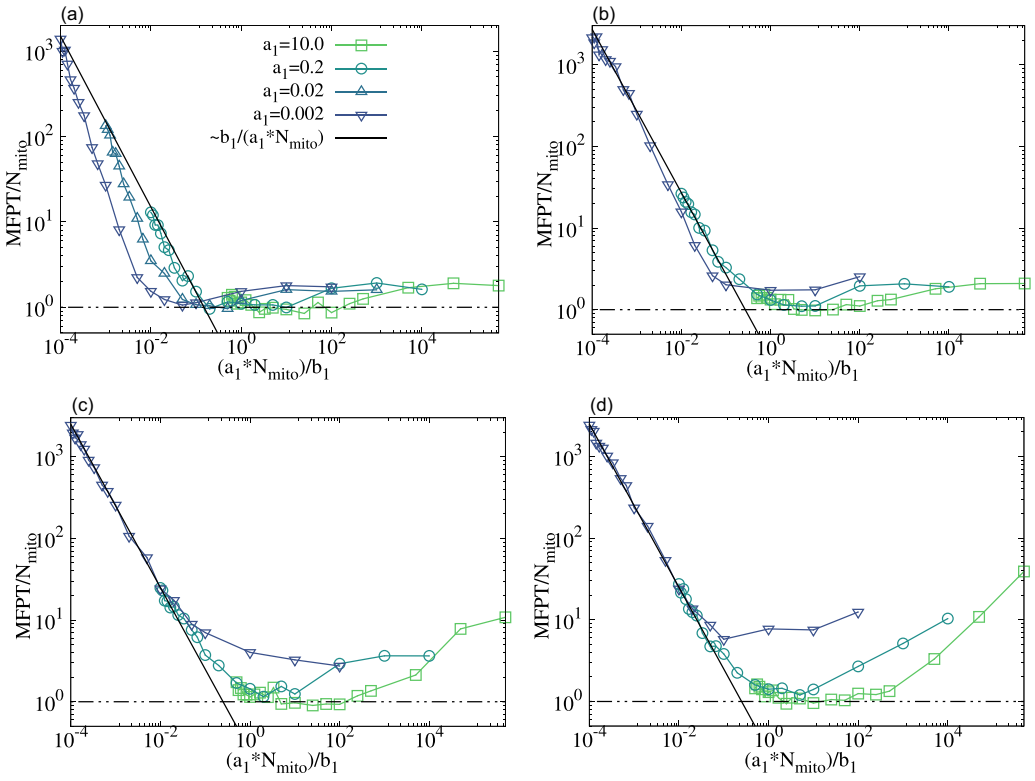

FIG. 11. Search times for particle diffusing on model aspatial dynamic mitochondrial network with variation in end-to-side fusion levels. MFPT of a particle to find a randomly selected mitochondrial fragment from an initial location on another randomly selected fragment, as the scaled ratio of end-to-end fusion to fission $a_1 N_{\text{mito}}/b_1$ is varied. End-to-side fusion rate varies between panels with (a) $a_2 = 10$, (b) $a_2 = 0.1$, (c) $a_2 = 0.001$, and (d) $a_2 = 0.000\,01$. The black solid line is $\sim b_1/(a_1 N_{\text{mito}})$ and the dot-dashed black line is minimum search time $\langle T_{\text{min}} \rangle$ from Eq. (4). Legend in (a) indicates end-to-end fusion rate a_1 and similarly applies to (b)–(d) except $a_1 = 0.02$ is absent from the latter panels. Across all panels, the rate to move to connected mitochondrial fragment is $k_m = 1$, the number of minimal mitochondrial fragments $N_{\text{mito}} = 50$, and data averaged over 100 samples.

Figs. 10(c) and 10(d). D_{eff} and MFPT differ more than for the networks with no restriction on node degree, with somewhat higher D_{eff} and lower MFPT for $m = 441$. However, both D_{eff} and MFPT are qualitatively similar to the networks in Fig. 2 with a maximum node degree of two that do not conserve mass. As for the networks with limited node degree $p \neq \lambda_{\text{add}}/(\lambda_{\text{add}} + \lambda_{\text{remove}})$, for the p in Eq. (A2) we use bond probability measured from simulations, rather than $\lambda_{\text{add}}/(\lambda_{\text{add}} + \lambda_{\text{remove}})$ as for the networks without node degree restrictions. The lattice spacing $L/(n-1)$ as $\lambda_{\text{add}}/(\lambda_{\text{add}} + \lambda_{\text{remove}})$ is varied as shown in insets of Figs. 10(b) and 10(d).

We attribute the relatively small differences between networks that do and do not conserve mass to finite size effects, since the effective diffusivity and MFPT for the higher mass system ($m = 625$) is closer to these quantities for the networks that do not conserve mass in Fig. 2.

2. Aspatial agent-based model

Figure 4(a) examines the MFPT for the aspatial agent-based dynamic mitochondrial network model for a branching network with intermediate end-to-side fusion rate $a_2 = 0.01$ and a nonbranching network with $a_2 = 0$. Figure 11 explores other a_2 values. For lower a_2 values [Figs. 11(c) and 11(d)] the MFPT trends toward the results for the nonbranching model [Fig. 4(a), dashed curves]. For higher a_2 values [Figs. 11(a) and 11(b)] the MFPT decreases below the MFPT $\sim b_1/(a_1 N_{\text{mito}})$ trend as branching fusions connecting short mitochondrial fragments and allows a particle to sample mitochondria rapidly. Since three-way junctions fission into a free end and a degree-two node at rate $b_2 = (3/2)b_1$, the high a_2 value allows the MFPT to decrease below the MFPT $\sim b_1/(a_1 N_{\text{mito}})$ trend.

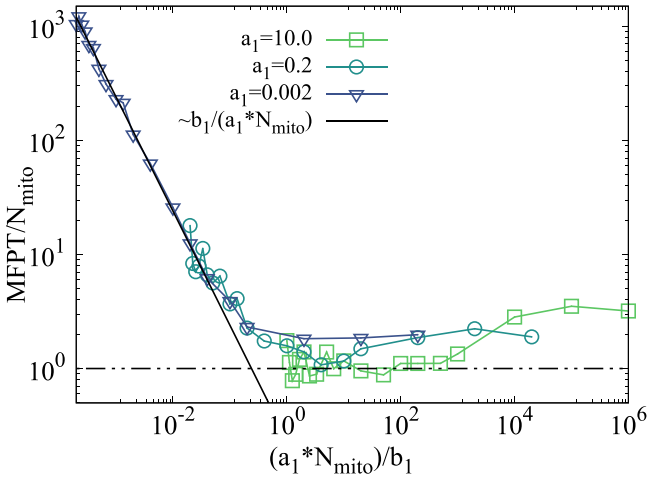

FIG. 12. Search times for particle diffusing on model aspatial dynamic mitochondrial network with larger network size. MFPT of a particle to find a randomly selected mitochondrial fragment from an initial location on another randomly selected fragment, as the scaled ratio of end-to-end fusion to fission $a_1 N_{\text{mito}}/b_1$ is varied. Black solid line is $\sim b_1/(a_1 N_{\text{mito}})$ and dot-dashed black line is minimum search time $\langle T_{\text{min}} \rangle$ from Eq. (4). Legend indicates end-to-end fusion rate a_1. $a_2 = 0.01$, the rate to move to connected mitochondrial fragments is $k_m = 1$, number of minimal mitochondrial fragments $N_{\text{mito}} = 100$ (in contrast to $N_{\text{mito}} = 50$ for other aspatial model results), and data averaged over 100 samples.

Figure 12 compares MFPT for a network with $N_{\text{mito}} = 100$ mitochondrial fragments instead of $N_{\text{mito}} = 50$ in Fig. 4(a), showing very similar scaled search times.

[1] B. Westermann, Mitochondrial fusion and fission in cell life and death, Nat. Rev. Mol. Cell Biol. **11**, 872 (2010).

[2] A. S. Monzel, J. A. Enríquez, and M. Picard, Multifaceted mitochondria: Moving mitochondrial science beyond function and dysfunction, Nature Metabolism **5**, 546 (2023).

[3] O. Bergman and D. Ben-Shachar, Mitochondrial oxidative phosphorylation system (oxphos) deficits in schizophrenia: possible interactions with cellular processes, Can. J. Psychiatry **61**, 457 (2016).

[4] M. Liesa, M. Palacín, and A. Zorzano, Mitochondrial dynamics in mammalian health and disease, Physiol. Rev. **89**, 799 (2009).

[5] J. Zhao, J. Zhang, M. Yu, Y. Xie, Y. Huang, D. W. Wolff, P. W. Abel, and Y. Tu, Mitochondrial dynamics regulates migration and invasion of breast cancer cells, Oncogene **32**, 4814 (2013).

[6] N. Exner, A. K. Lutz, C. Haass, and K. F. Winklhofer, Mitochondrial dysfunction in Parkinson's disease: molecular mechanisms and pathophysiological consequences, The EMBO J. **31**, 3038 (2012).

[7] E. Tönnies and E. Trushina, Oxidative stress, synaptic dysfunction, and Alzheimer's disease, J. Alzheimer's Dis. **57**, 1105 (2017).

[8] V. M. Sukhorukov, D. Dikov, A. S. Reichert, and M. Meyer-Hermann, Emergence of the mitochondrial reticulum from fission and fusion dynamics, PLoS Comput. Biol. **8**, e1002745 (2012).

[9] M. P. Viana, A. I. Brown, I. A. Mueller, C. Goul, E. F. Koslover, and S. M. Rafelski, Mitochondrial fission and fusion dynamics generate efficient, robust, and evenly distributed network topologies in budding yeast cells, Cell Systems **10**, 287 (2020).

[10] A. I. Brown, L. M. Westrate, and E. F. Koslover, Impact of global structure on diffusive exploration of organelle networks, Sci. Rep. **10**, 4984 (2020).

[11] G. R. Lewis and W. F. Marshall, Mitochondrial networks through the lens of mathematics, Phys. Biol. **20**, 051001 (2023).

[12] T. Kleele, T. Rey, J. Winter, S. Zaganelli, D. Mahecic, H. Perreten Lambert, F. P. Ruberto, M. Nemir, T. Wai, T. Pedrazzini *et al.*, Distinct fission signatures predict mitochondrial degradation or biogenesis, Nature (London) **593**, 435 (2021).

[13] M. Liesa and O. S. Shirihai, Mitochondrial dynamics in the regulation of nutrient utilization and energy expenditure, Cell Metab. **17**, 491 (2013).

[14] S. Campello, R. A. Lacalle, M. Bettella, S. Mañes, L. Scorrano, and A. Viola, Orchestration of lymphocyte chemotaxis by mitochondrial dynamics, J. Exp. Med. **203**, 2879 (2006).

[15] B. J. Seo, S. H. Yoon, and J. T. Do, Mitochondrial dynamics in stem cells and differentiation, Int. J. Mol. Sci. **19**, 3893 (2018).

[16] S. Hoppins, L. Lackner, and J. Nunnari, The machines that divide and fuse mitochondria, Annu. Rev. Biochem. **76**, 751 (2007).

[17] R. E. Jensen, A. E. Aiken Hobbs, K. L. Cerveny, and H. Sesaki, Yeast mitochondrial dynamics: fusion, division, segregation, and shape, Microsc. Res. Tech. **51**, 573 (2000).

[18] Z. Wang, P. Natekar, C. Tea, S. Tamir, H. Hakozaki, and J. Schöneberg, Mitotnt: Mitochondrial temporal network tracking for 4D live-cell fluorescence microscopy data, PLoS Comput. Biol. **19**, e1011060 (2023).

[19] K. Holt, J. Winter, S. Manley, and E. F. Koslover, Spatiotemporal modeling of mitochondrial network architecture bioRxiv 2024.01.24.577101 (2024).

[20] A. R. Fenton, T. A. Jongens, and E. L. Holzbaur, Mitochondrial dynamics: Shaping and remodeling an organelle network, Curr. Opin. Cell Biol. **68**, 28 (2021).

[21] P. K. Patel, O. Shirihai, and K. C. Huang, Optimal dynamics for quality control in spatially distributed mitochondrial networks, PLoS Comput. Biol. **9**, e1003108 (2013).

[22] M. Guo, A. J. Ehrlicher, M. H. Jensen, M. Renz, J. R. Moore, R. D. Goldman, J. Lippincott-Schwartz, F. C. Mackintosh, and D. A. Weitz, Probing the stochastic, motor-driven properties of the cytoplasm using force spectrum microscopy, Cell **158**, 822 (2014).

[23] J. M. Chustecki, D. J. Gibbs, G. W. Bassel, and I. G. Johnston, Network analysis of arabidopsis mitochondrial dynamics reveals a resolved tradeoff between physical distribution and social connectivity, Cell Systems **12**, 419 (2021).

[24] R. Rossignol, R. Gilkerson, R. Aggeler, K. Yamagata, S. J. Remington, and R. A. Capaldi, Energy substrate modulates mitochondrial structure and oxidative capacity in cancer cells, Cancer Res. **64**, 985 (2004).

[25] A. J. Molina, J. D. Wikstrom, L. Stiles, G. Las, H. Mohamed, A. Elorza, G. Walzer, G. Twig, S. Katz, B. E. Corkey *et al.*, Mitochondrial networking protects β-cells from nutrient-induced apoptosis, Diabetes **58**, 2303 (2009).

[26] L. C. Gomes, G. D. Benedetto, and L. Scorrano, During autophagy mitochondria elongate, are spared from degradation and sustain cell viability, Nat. Cell Biol. **13**, 589 (2011).

[27] S. M. Rafelski, Mitochondrial network morphology: building an integrative, geometrical view, BMC Biol. **11**, 71 (2013).

[28] H. Zhang, K. J. Menzies, and J. Auwerx, The role of mitochondria in stem cell fate and aging, Development **145**, dev143420 (2018).

[29] T. Tsuboi, M. P. Viana, F. Xu, J. Yu, R. Chanchani, X. G. Arceo, E. Tutucci, J. Choi, Y. S. Chen, R. H. Singer *et al.*, Mitochondrial volume fraction and translation duration impact mitochondrial mrna localization and protein synthesis, Elife **9**, e57814 (2020).

[30] G. López-Doménech and J. T. Kittler, Mitochondrial regulation of local supply of energy in neurons, Curr. Opin. Neurobiol. **81**, 102747 (2023).

[31] H. Hoitzing, I. G. Johnston, and N. S. Jones, What is the function of mitochondrial networks? a theoretical assessment of hypotheses and proposal for future research, BioEssays **37**, 687 (2015).

[32] J. M. Chustecki and I. G. Johnston, Collective mitochondrial dynamics resolve conflicting cellular tensions: From plants to general principles, in *Seminars in Cell & Developmental Biology* (Elsevier, New York, 2024), Vol. 156, pp. 253–265

[33] I. Scott and R. J. Youle, Mitochondrial fission and fusion, Essays Biochem. **47**, 85 (2010).

[34] C.-R. Chang and C. Blackstone, Dynamic regulation of mitochondrial fission through modification of the dynamin-related protein Drp1, Ann. N.Y. Acad. Sci. **1201**, 34 (2010).

[35] C. C. Williams, C. H. Jan, and J. S. Weissman, Targeting and plasticity of mitochondrial proteins revealed by proximity-specific ribosome profiling, Science **346**, 748 (2014).

[36] X. G. Arceo, E. F. Koslover, B. M. Zid, and A. I. Brown, Mitochondrial mRNA localization is governed by translation kinetics and spatial transport, PLoS Comput. Biol. **18**, e1010413 (2022).

[37] A. H. Khan, X. Gu, R. J. Patel, P. Chuphal, M. P. Viana, A. I. Brown, B. M. Zid, and T. Tsuboi, Mitochondrial protein heterogeneity stems from the stochastic nature of co-translational protein targeting in cell senescence, Nat. Commun. **15**, 8274 (2024).

[38] J. M. Palozzi, S. P. Jeedigunta, and T. R. Hurd, Mitochondrial DNA purifying selection in mammals and invertebrates, J. Mol. Biol. **430**, 4834 (2018).

[39] T. Ono, K. Isobe, K. Nakada, and J.-I. Hayashi, Human cells are protected from mitochondrial dysfunction by complementation of DNA products in fused mitochondria, Nat. Genet. **28**, 272 (2001).

[40] M. P. Viana, S. Lim, and S. M. Rafelski, Quantifying mitochondrial content in living cells, in *Methods in Cell Biology* (Elsevier, Amsterdam, 2015), Vol. 125, pp. 77–93.

[41] F. M. Fazal, S. Han, K. R. Parker, P. Kaewsapsak, J. Xu, A. N. Boettiger, H. Y. Chang, and A. Y. Ting, Atlas of subcellular RNA localization revealed by APEX-Seq, Cell **178**, 473 (2019).

[42] H. S. Ilamathi, M. Ouellet, R. Sabouny, J. Desrochers-Goyette, M. A. Lines, G. Pfeffer, T. E. Shutt, and M. Germain, A new automated tool to quantify nucleoid distribution within mitochondrial networks, Sci. Rep. **11**, 22755 (2021).

[43] N. Zamponi, E. Zamponi, S. A. Cannas, O. V. Billoni, P. R. Helguera, and D. R. Chialvo, Mitochondrial network complexity emerges from fission/fusion dynamics, Sci. Rep. **8**, 363 (2018).

[44] N. Zamponi, E. Zamponi, S. A. Cannas, and D. R. Chialvo, Universal dynamics of mitochondrial networks: A finite-size scaling analysis, Sci. Rep. **12**, 17074 (2022).

[45] V. M. Sukhorukov and M. Meyer-Hermann, Structural heterogeneity of mitochondria induced by the microtubule cytoskeleton, Sci. Rep. **5**, 13924 (2015).

[46] K. Giannakis, J. M. Chustecki, and I. G. Johnston, Exchange on dynamic encounter networks allows plant mitochondria to collect complete sets of mitochondrial dna products despite their incomplete genomes, Quant. Plant Biol. **3**, e18 (2022).

[47] A. K. Harrison and R. Zwanzig, Transport on a dynamically disordered lattice, Phys. Rev. A **32**, 1072 (1985).

[48] M. Sahimi, Dynamic percolation and diffusion in disordered systems, J. Phys. C **19**, 1311 (1986).

[49] C. D. Levermore, W. Nadler, and D. L. Stein, Random walks on a fluctuating lattice: A renormalization group approach applied in one dimension, Phys. Rev. E **51**, 2779 (1995).

[50] G. J. Lapeyre, Random walks on a fluctuating lattice, Ph.D. thesis, The University of Arizona, 2001.

[51] J. A. Revelli, C. E. Budde, and H. S. Wio, Diffusion in fluctuating media: First passage time problem, Phys. Lett. A **306**, 104 (2002).

[52] T. Hoffmann, M. A. Porter, and R. Lambiotte, Generalized master equations for non-poisson dynamics on networks, Phys. Rev. E **86**, 046102 (2012).

[53] D. T. Gillespie, Exact stochastic simulation of coupled chemical reactions, J. Phys. Chem. **81**, 2340 (1977).

[54] D. Stauffer and A. Aharony, *Introduction to Percolation Theory* (CRC Press, Boca Raton, 2018).

[55] V. Wilkens, W. Kohl, and K. Busch, Restricted diffusion of oxphos complexes in dynamic mitochondria delays their exchange between cristae and engenders a transitory mosaic distribution, J. Cell Sci. **126**, 103 (2013).

[56] X. Liu, D. Weaver, O. Shirihai, and G. Hajnóczky, Mitochondrial "kiss-and-run": interplay between mitochondrial motility and fusion–fission dynamics, EMBO J. **28**, 3074 (2009).

[57] A. Agrawal and E. F. Koslover, Optimizing mitochondrial maintenance in extended neuronal projections, PLoS Comput. Biol. **17**, e1009073 (2021).

[58] C. Jakubke, R. Roussou, A. Maiser, C. Schug, F. Thoma, D. Bunk, D. Hörl, H. Leonhardt, P. Walter, T. Klecker *et al.*, Cristae-dependent quality control of the mitochondrial genome, Sci. Adv. **7**, eabi8886 (2021).

[59] V. M. Sukhorukov, D. Dikov, K. Busch, V. Strecker, I. Wittig, and J. Bereiter-Hahn, Determination of protein mobility in mitochondrial membranes of living cells, Biochim. Biophys. Acta, Biomembr. **1798**, 2022 (2010).

[60] M. Pósfai, B. Szegedy, I. Bačić, L. Blagojević, M. Abért, J. Kertész, L. Lovász, and A.-L. Barabási, Impact of physicality on network structure, Nat. Phys. **20**, 142 (2024).

[61] D. J. Watts and S. H. Strogatz, Collective dynamics of "small-world" networks, Nature (London) **393**, 440 (1998).

[62] J. D. Noh and H. Rieger, Random walks on complex networks, Phys. Rev. Lett. **92**, 118701 (2004).

[63] N. Masuda, M. A. Porter, and R. Lambiotte, Random walks and diffusion on networks, Phys. Rep. **716-717**, 1 (2017).

[64] https://github.com/aidanbrowntmu/mitobranching.